ENVIRONMENTAL RESEARCH
LETTERS

PURPOSE-LED PUBLISHING™
Celebrating the 20th anniversary of Environmental Research Letters

LETTER • **OPEN ACCESS**

Contrasting hydroclimate variations across inner Asian drylands in a warming climate

To cite this article: Shanshan Wang *et al* 2026 *Environ. Res. Lett.* **21** 154045

View the article online for updates and enhancements.

You may also like

- Distinct vegetation response to drying and wetting trends across an aridity threshold
Wei Zhao, Xiubo Yu, Yu Liu et al.
- The PMIP4 simulated dryland aridity changes during the Last Interglacial
Shanshan Liu and Xuecheng Zhou
- Precipitation leads the long-term vegetation increase in the conterminous United States drylands
Yuhe Chang, Alexander J Winkler, Amirhossein Noori et al.

This content was downloaded from IP address 202.201.10.3 on 10/11/2026 at 09:55

ENVIRONMENTAL RESEARCH
LETTERS

Check for updates

OPEN ACCESS

RECEIVED
12 March 2026

REVISED
4 July 2026

ACCEPTED FOR PUBLICATION
22 July 2026

PUBLISHED
12 August 2026

Original content from this work may be used under the terms of the Creative Commons Attribution 4.0 licence.

Any further distribution of this work must maintain attribution to the author(s) and the title of the work, journal citation and DOI.

LETTER

Contrasting hydroclimate variations across inner Asian drylands in a warming climate

Shanshan Wang[1,2], **Yuanyuan Hu**[1], **Hao Wang**[1], **Dongyu He**[1] **and Jianping Huang**[1,2,*]

[1] Key Laboratory for Semi-Arid Climate Change of the Ministry of Education, College of Atmospheric Sciences, Lanzhou University, Lanzhou, People's Republic of China
[2] Collaborative Innovation Center for Western Ecological Safety, Lanzhou, People's Republic of China
[*] Author to whom any correspondence should be addressed.

E-mail: hjp@lzu.edu.cn

Keywords: surface water availability, drylands of East and Central Asia, spatial heterogeneity, soil moisture

Abstract

Under future climate warming, surface water availability (precipitation minus evapotranspiration, *P–E*) over the drylands of East and Central Asia shows a pronounced contrasting response by the late 21st century relative to the historical reference period. East Asian drylands, as the core of Northwest China's warming and wetting trend, tend to become wetter with increased *P–E*, while adjacent Central Asian drylands undergo drying with reduced *P–E*. To elucidate the underlying mechanisms, we analyze CMIP6 simulations combined with LFMIP-pdLC experiments to disentangle the feedback effects associated with soil moisture (SM) and non-SM processes. Our results demonstrate that this opposing hydroclimatic pattern is predominantly controlled by non-SM feedbacks. In East Asia, a strengthened East Asian summer monsoon circulation substantially enhances precipitation, whose increase exceeds the concurrent rise in evapotranspiration. In Central Asia, westerly-related rainfall increases only modestly, while amplified evapotranspiration driven by elevated vapor pressure deficits dominates the moisture budget. SM feedback acts as a damping factor that modulates both thermodynamic and dynamic components of the moisture budget, thereby partially offsetting non-SM effects and alleviating the regional imbalance in *P–E* distribution. These findings advance the mechanistic understanding of dryland hydroclimate change and provide a scientific basis for regionally differentiated water resource planning and adaptation under future warming.

1. Introduction

In drylands, the availability of surface water, quantified as precipitation minus evapotranspiration (*P–E*), is a critical metric for assessing moisture levels (Zhang *et al* 2023, Gu *et al* 2025). This crucial balance is influenced by a range of interconnected factors. These include soil moisture (SM), the East Asian summer monsoon (EASM), westerly winds, vapor pressure deficit (VPD), and vegetation characteristics like leaf area index (LAI). Together, they shape regional water budgets by directly affecting precipitation and evapotranspiration, as well as atmospheric moisture transport (Alessi *et al* 2022, Qiao *et al* 2023, Yuan *et al* 2023, Zhu and Liu 2023, Chen *et al* 2024, Li *et al* 2024b, Hu *et al* 2025b).

Specifically, SM plays a key role in regulating local water inflow. By altering the stability of the near-surface atmosphere through latent and sensible heat fluxes, SM directly influences local precipitation and, consequently, *P–E* (Zeng *et al* 2019, Seo and Ha 2022). For instance, reduced SM can suppress precipitation while simultaneously increasing evapotranspiration. This leads to a decline in *P–E* and can accelerate the onset of flash droughts (Wang and Yuan 2022). Conversely, substantial moisture advection, often associated with specific large-scale circulation patterns, can generate ample precipitation. This boosts *P–E* and supports ecosystem stability (Li *et al* 2017, Yuan *et al* 2023, Wang and Wu 2024). Concurrently, VPD and LAI are critical controllers of evapotranspiration. Higher VPD results in drier

© 2026 The Author(s). Published by IOP Publishing Ltd

air, while a greater LAI signifies expanded vegetation cover. Both collectively amplify the atmosphere's evaporative demand, further shaping the variability of *P–E* (Yang *et al* 2023, Lin *et al* 2025).

While broad patterns of spatial heterogeneity across global drylands have been established—particularly the fundamental division between nearshore and inland areas (Hu *et al* 2025a)—applying this large-scale understanding to explain finer-scale, intra-regional dynamics presents a significant challenge. Observational evidence has further revealed notable internal differences within inland drylands, specifically between the drylands of Central Asia and East Asia, even in their SM change trends (Hu *et al* 2025a). Against the backdrop of Northwest China's well-documented warming and wetting, a key and unresolved question arises over why the adjacent Central Asian drylands exhibit contrasting moisture dynamics while the East Asian drylands, the core of this warming and wetting trend, experience increased moisture. These observed heterogeneities raise critical questions about how *P–E* will evolve in inland drylands under global warming, whether these regional differences in *P–E* dynamics and their environmental responses will persist, and what distinct mechanisms drive these divergent variations across East and Central Asian drylands.

Answering these questions is particularly pressing. The drylands of East and Central Asia form a core arid and semi-arid zone in the Northern Hemisphere. This region is characterized by high population density in key subregions, pronounced ecological vulnerability due to fragile water and soil resources, strong spatiotemporal gradients in climate and land use, and a unique hydrological sensitivity to the interplay between the EASM and the westerlies (Sardans *et al* 2024, Li *et al* 2024a, Ma *et al* 2025).

Does the *P–E* in the drylands of East and Central Asia exhibit spatial heterogeneity? Although numerous factors influencing *P–E* have been proposed, their specific roles in driving these regional patterns remain inadequately quantified. To address this, our study integrates CMIP6 and LFMIP-pdLC model experiments with atmospheric moisture budget diagnostics. This approach allows us to define key circulation indices (e.g. EASM Index (EASMI), westerly index (WI)) and systematically attribute the observed *P–E* heterogeneities to their dynamic and thermodynamic drivers. Our findings will provide not only a mechanistic understanding of dryland hydroclimatology but also critical evidence for guiding local water-cycle management. Specifically, they can inform strategies for enhancing water security, allocating resources effectively under a changing climate, and maintaining ecosystem resilience in these vulnerable, populous regions, thereby supporting sustainable development goals (Abbott *et al* 2019).

2. Data and method

2.1. Data

In this study, we used monthly data from six CMIP6 models over 35–50° N, 50–125° E, covering both the historical (1980–2014) and future (2066–2100, SSP585 scenario) periods. The data were interpolated onto a common grid of 1.875° × 2.5° using linear interpolation. Our analysis is based on the six models for which both the standard CMIP6 simulations and the corresponding LFMIP-pdLC experiments, together with the required variables, are available. The CMIP6 ensemble members used are CESM2 (r4i1p1f1), CMCC-ESM2 (r1i1p1f1), CNRM-CM6-1 (r1i1p1f2), EC-Earth3 (r1i1p1f1), IPSL-CM6A-LR (r1i1p1f1), and MPI-ESM1-2-LR (r1i1p1f1), which have also been shown to perform well in simulating variables such as SM and *P–E* (Zhou *et al* 2021, 2022, Qiao *et al* 2023). The analyzed variables include precipitation (pr), moisture in the upper portion of the soil column (mrsos, 0–10 cm), latent heat flux (hfls), air temperature (tas), near-surface relative humidity (hurs), eastward wind (ua), northward wind (va), and leaf area index (lai). Since not all models provide evapotranspiration data, we calculated evapotranspiration from air temperature (T) and latent heat flux (LE). The specific formula is as follows (Allen *et al* 1998):

$$E = \frac{\mathrm{LE}}{2.501 - \left(2.361 * 10^{-3}\right) T} \tag{1}$$

where the unit of T is degrees Celsius.

2.2. Study area

In this paper, our study area focuses on the drylands of East and Central Asia (35–50° N, 50–125° E) excluding the Qinghai-Tibet Plateau. As one of the world's most populous drylands (Ma *et al* 2025), changes in *P–E* in this region are closely tied to ecological security and the survival and development of local populations (Seddon *et al* 2016). To better study variations in *P–E*, we have divided the region into Central Asia and East Asia. We use 80° E as a simple boundary to distinguish Central Asia from East Asia, defining Central Asia as the region between 35–50° N and 50–80° E, and East Asia as 35–50° N, 80–125° E, a demarcation whose validity for our conclusions has been confirmed regardless of whether administrative or geographical boundaries are employed. Within this context, drylands are defined as regions with an aridity index (AI) of 0.65 or less (Middleton and Thomas 1997, Li *et al* 2015), provided by the third edition of the global desiccation index and potential evapotranspiration database from Plant Data Center of Chinese Academy of Sciences (Trabucco and Zomer 2008, 2019, Zomer *et al* 2022).

2.3. SM-atmosphere feedback experiments

This study employs the output results of the Land Feedback Model Intercomparison Project with prescribed Land Conditions (LFMIP-pdLC, Hurk *et al* 2016), where the land conditions are prescribed as the annual mean cycle simulated by historical global climate models from 1980 to 2014. By comparing the fully coupled CMIP6 simulations with the corresponding LFMIP-pdLC simulations, we estimate the contribution of SM feedback to changes in *P–E*.

Within this framework, the response in LFMIP-pdLC is used to represent the component of climate change that occurs without interactive SM variability (hereafter referred to as the non-SM effect, Song *et al* 2025). This non-SM effect should not be interpreted as a single physical process; rather, it reflects the combined influence of atmospheric thermodynamic changes, large-scale circulation changes, and land-surface responses other than interactive SM variability. In this study, we focus in particular on circulation-related changes associated with moisture transport, as well as land-surface factors closely linked to evapotranspiration, including VPD and LAI.

2.4. Moisture budget decomposition

Following previous studies (Zhou *et al* 2022, Hu *et al* 2025a), precipitation (P) is decomposed into evapotranspiration (E) and moisture convergence (MC):

$$P = E + \mathrm{MC}. \tag{2}$$

The moisture convergence is defined as the negative divergence of the vertically integrated moisture flux:

$$\mathrm{MC} = -\frac{1}{\rho_w g}\nabla \cdot \int_0^{p_s} (uq)\,\mathrm{d}p \tag{3}$$

where ρ_w is the density of water, g is gravitational acceleration, ∇ is the horizontal divergence operator, u is the horizontal wind vector, and q is specific humidity. Based on the mass continuity equation (Bony *et al* 2013), the change in moisture convergence between the future and historical periods is approximated as:

$$\begin{aligned}\Delta\mathrm{MC} \approx & -\frac{1}{\rho_w g}\nabla \cdot \int_0^{p_s} (\overline{u_0}\cdot\Delta\bar{q} + \Delta\bar{u}\cdot\Delta\bar{q})\,\mathrm{d}p \\ & -\frac{1}{\rho_w g}\nabla \cdot \int_0^{p_s} \left(\Delta\overline{\omega}\cdot\frac{\partial q}{\partial p}\right)\mathrm{d}p\end{aligned} \tag{4}$$

where ω is the pressure vertical velocity. According to the above equations, ΔMC consists of three components: the thermodynamic term $(-\frac{1}{\rho_w g}\nabla \cdot \int_0^{p_s} (\overline{u_0}\cdot\Delta\bar{q})\,\mathrm{d}p)$, the dynamic term $(-\frac{1}{\rho_w g}\nabla \cdot \int_0^{p_s} \left(\Delta\overline{\omega}\cdot\frac{\partial q}{\partial p}\right)\mathrm{d}p)$, and the nonlinear term $(-\frac{1}{\rho_w g}\nabla \cdot \int_0^{p_s} (\Delta\bar{u}\cdot\Delta\bar{q})\,\mathrm{d}p)$.

2.5. EASMI and WI

In this paper, to further research the influencing factors of precipitation changes in Central and East Asia, we define EASMI and WI and analyze their trend changes. EASMI and WI are defined as regional averages of 850 hPa and 500 hPa zonal winds, respectively. EASMI is calculated based on the June-August mean winds over 22.5–40° N and 105–120° E, whereas WI is derived using the annual mean winds over 35–50° N and 50–80° E (Li *et al* 2019).

2.6. VPD

To investigate the factors affecting evapotranspiration, we study VPD, whose relevant calculation formula is as follows (Lin *et al* 2025):

$$\mathrm{VPD} = 6.112 \cdot \exp\left(\frac{17.67 \cdot \mathrm{tas}}{\mathrm{tas} + 243.5}\right) \cdot (1 - \mathrm{hurs}/100)\,. \tag{5}$$

3. Results

3.1. Future changes in key factors of the water cycle in Central Asia and East Asia

Future projections indicate that the variation of *P–E* in Central Asia and East Asia will exhibit significant spatial heterogeneity (figure 1(a)). As shown, *P–E* exhibits opposing trends across the regions, decreasing in Central Asia and increasing in East Asia concurrently. This change is primarily driven by non-SM effect, while SM effect partially offsets the impact of non-SM effect (figures 1(d) and (g)). Furthermore, this phenomenon occurs primarily because non-SM effect and SM effect influence the distribution of precipitation and evapotranspiration in the local area.

Under the influence of non-SM effect, both precipitation and evapotranspiration exhibit an overall upward trend (figures 1(e) and (f)). However, their spatial patterns are converse: precipitation increases more in East Asia than in Central Asia, whereas evapotranspiration shows a larger increase in Central Asia. Consequently, *P–E* diminishes in Central Asia but is amplified in East Asia, thereby exacerbating water stress in the former and alleviating aridification in the latter. Additionally, under the influence of SM effect, both precipitation and evapotranspiration decrease in Central Asia (figures 1(h) and (i)). However, the decrease in precipitation is less pronounced than that in evapotranspiration, resulting in a net increase of *P–E* in Central Asia (figure 1(g)). In contrast, over East Asia, precipitation shows only a slight increase, which is much smaller than the increase in evapotranspiration, leading to a net decrease in *P–E*. These results indicate that the spatial heterogeneity of *P–E* arises from regionally distinct responses of precipitation and evapotranspiration to the non-SM and SM effects, as well as from differences in their relative magnitudes. Therefore, to better understand the

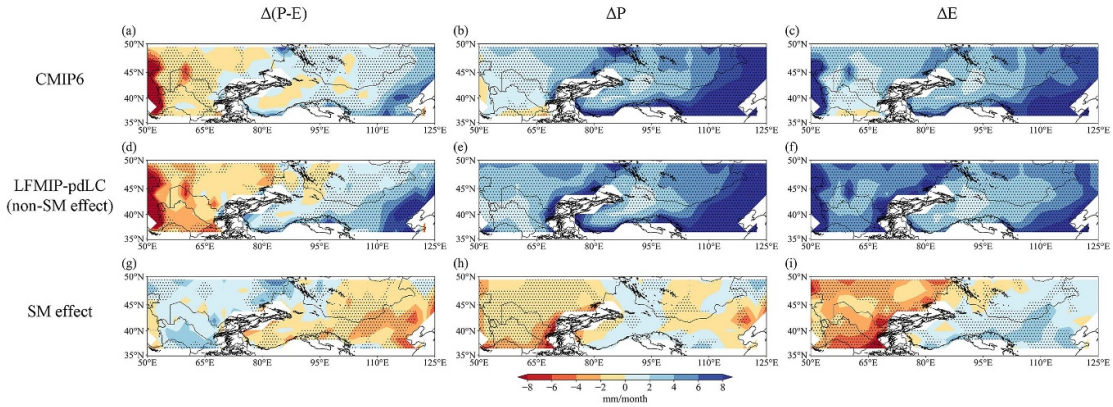


Figure 1. Future multi-model average changes in surface water availability, precipitation and evapotranspiration in Central Asia and East Asia. (a)–(c) Multi-model average changes in $P–E$ ($\Delta(P–E)$), precipitation (ΔP) and evapotranspiration (ΔE) between 1980–2014 (historical simulation) and 2066–2100 (SSP585 simulation) in the six CMIP6 models. The dotted areas indicate that the sign of changes in $\Delta(P–E)$, ΔP, and ΔE aligns with the sign of changes in the multi-model average (as shown in the figure), and this consistency is maintained in at least four out of six models. (d)–(f) and (g)–(i) are similar to (a)–(c) but are based on non-SM effect (results from LFMIP-pdLC experiment) and on SM effect (results from CMIP6 minus LFMIP-pdLC experiment), respectively.

mechanisms behind the spatial heterogeneity of $P–E$, it is necessary to further investigate the physical processes responsible for the precipitation and evapotranspiration changes associated with the non-SM and SM effects.

3.2. The mechanism of SM effect's influence on P–E

To further explore the mechanism, we first examine the spatial variation in SM, which reveals that it closely mirrors the distributions of precipitation and evapotranspiration (figure 2(a)). This correspondence suggests that SM is a key intermediary linking land-surface change to hydroclimatic responses (Jiang *et al* 2023, Zhang *et al* 2025, Hu *et al* 2025b). To further diagnose how the SM effect influences $P–E$, we analyze the atmospheric moisture budget over Central Asia and East Asia (figures 2(b) and (c)), together with changes in moisture flux divergence and vertical motion (figures 2(d) and (e)).

The mechanism of the SM effect differs regionally. In Central Asia, reduced SM suppresses evapotranspiration, but $P–E$ nevertheless increases because moisture convergence strengthens sufficiently to offset the precipitation decline (figure 2(b)). This increase is dominated by the thermodynamic component of moisture convergence, suggesting that SM-induced changes in surface energy partitioning and near-surface temperature-humidity conditions favor stronger water-vapor transport into the region. Consistent with this interpretation, figure 2(d) shows enhanced moisture-flux convergence over Central Asia. Figure 2(e) further indicates that although subsidence strengthens in the mid-troposphere, this dynamic effect only partly offsets the enhanced low-level moisture supply, so the net SM effect remains an increase in $P–E$.

In contrast, in East Asia, the SM effect reduces $P–E$ by enhancing evapotranspiration while weakening moisture convergence (figure 2(c)). Here, the convergence reduction arises from both thermodynamic and dynamic contributions, indicating that SM anomalies affect not only the moisture-holding capacity of the atmosphere but also the circulation conditions governing moisture transport. The increased moisture-flux divergence over East Asia in figure 2(d) is consistent with this reduced convergence. These moisture budget diagnostics collectively explain why the SM effect produces opposite $P–E$ responses in the two regions and support the spatial pattern shown in figure 1(g).

3.3. The mechanism of non-SM effect's influence on P–E

Previous studies have shown that SM effect influences precipitation primarily by mediating moisture convergence and evapotranspiration, thereby modulating the local $P–E$. In our results, however, the non-SM effect is the dominant contributor to the contrasting $P–E$ changes between Central Asia and East Asia. Because the non-SM effect in the LFMIP-pdLC framework represents the response that occurs without interactive SM variability, it may include multiple physical processes. Here, rather than attempting a full process-level attribution, we examine several physically relevant pathways through which it may influence precipitation and evapotranspiration, focusing on atmospheric circulation, atmospheric evaporative demand, and vegetation change (Yang *et al* 2023).

Precipitation in Central Asia is primarily transported by westerlies, while in East Asia it is largely driven by the EASM (Cui *et al* 2021, Zhang *et al* 2022). We therefore examined WI for Central Asia and EASMI for East Asia under the non-SM effect (figures 3(a) and (b)). Notably, both EASMI and WI exhibit significant upward trends, with a stronger increase in EASMI. This result is consistent with

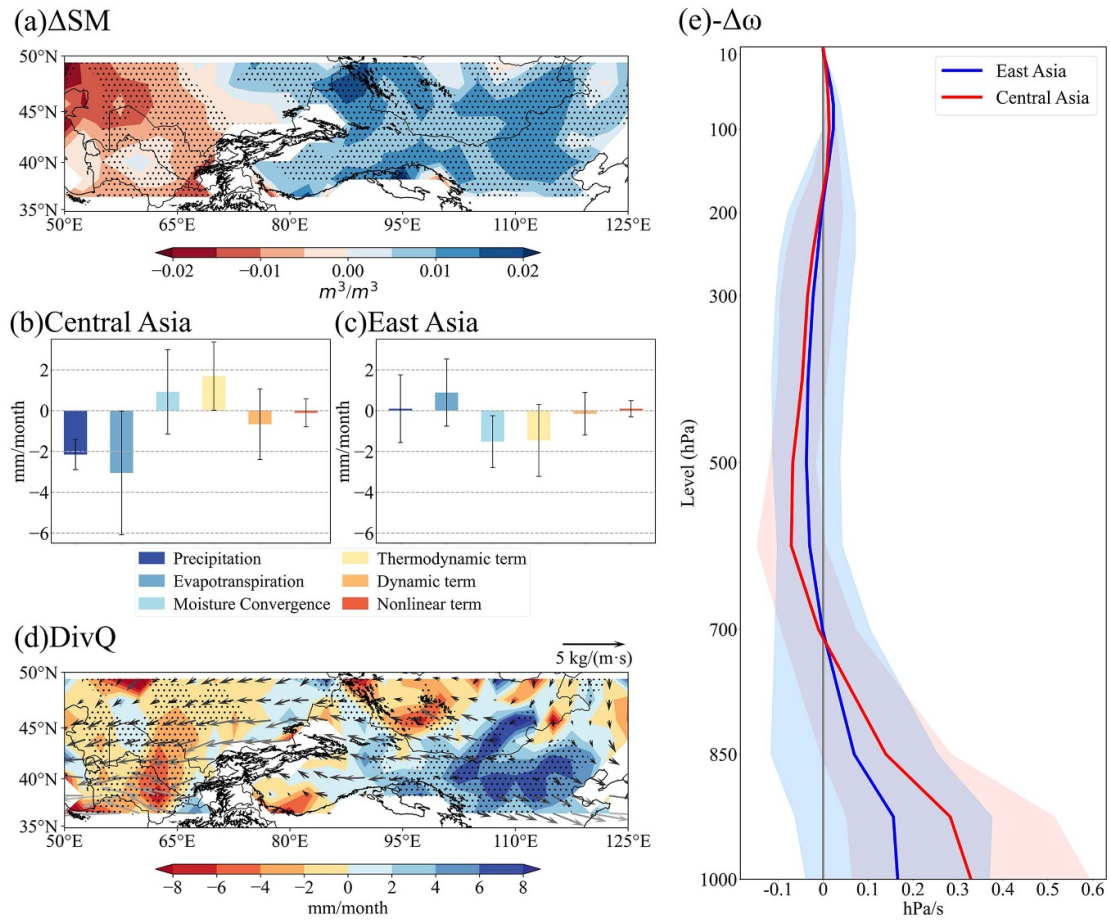


Figure 2. Mechanisms of SM effect on precipitation and evapotranspiration in Central Asia and East Asia. (a) Multi-model average changes in SM (ΔSM) between 1980–2014 (historical simulation) and 2066–2100 (SSP585 simulation) in the six CMIP6 models. (b) SM effect on changes in precipitation, evapotranspiration, moisture convergence, and the thermodynamic, dynamic, and nonlinear terms of moisture convergence in Central Asia between 1980–2014 and 2066–2100. (c) The same as (b) but for East Asia. (d) The same as (a) but for changes in water vapor flux divergence (ΔdivQ, color shading) and water vapor flux (vector). The dotted areas in (a) and (d) indicate that the sign of changes in ΔSM and ΔdivQ aligns with the sign of changes in the multi-model average (as shown in the figure), and this consistency is maintained in at least four out of six models. (e) SM effects on negative pressure velocity ($-\Delta\omega$) over Central Asia and East Asia. The error bar in (b), (c) and the shading in (e) show the standard deviation of each variable in the six models.

enhanced precipitation in both regions, especially in East Asia. The horizontal wind fields further support this interpretation (figures 3(c) and (d)). Central Asia shows strengthened westerly flow, while East Asia exhibits anomalous easterly flow together with enhanced monsoonal circulation. Although both circulation changes imply enhanced moisture transport, the resulting precipitation response is stronger in East Asia than in Central Asia. This contrast arises primarily because the enhancement of the EASM is stronger than that of the westerlies, leading to a larger circulation-driven increase in precipitation over East Asia. In addition, the East Asian monsoon delivers abundant oceanic moisture into the region, making the moisture supply more conducive to precipitation increases. By comparison, the increase in moisture transport associated with strengthened westerlies over Central Asia appears less efficient in generating precipitation. This difference is particularly evident in the eastern part of the East Asian drylands, which lies within the monsoon transition zone and is therefore especially sensitive to changes in monsoonal moisture transport.

To understand the evapotranspiration response under the non-SM effect, we further examine VPD and LAI (figures 3(e) and (f)). The widespread warming trend has increased atmospheric water-holding capacity and air dryness, as indicated by a pronounced rise in the VPD. As seen in figures 3(e) and (f), VPD increases markedly across the study region, with the strongest rise occurring in Central Asia, indicating enhanced atmospheric evaporative demand under warming. Such changes are consistent with stronger evapotranspiration, particularly in arid and semi-arid environments where atmospheric demand can exert strong control on water loss (Yuan *et al* 2025). Meanwhile, LAI also increases, with more pronounced greening in East Asia. This pattern is consistent with enhanced vegetation activity and transpiration, which can further increase evapotranspiration where vegetation cover is sufficient.

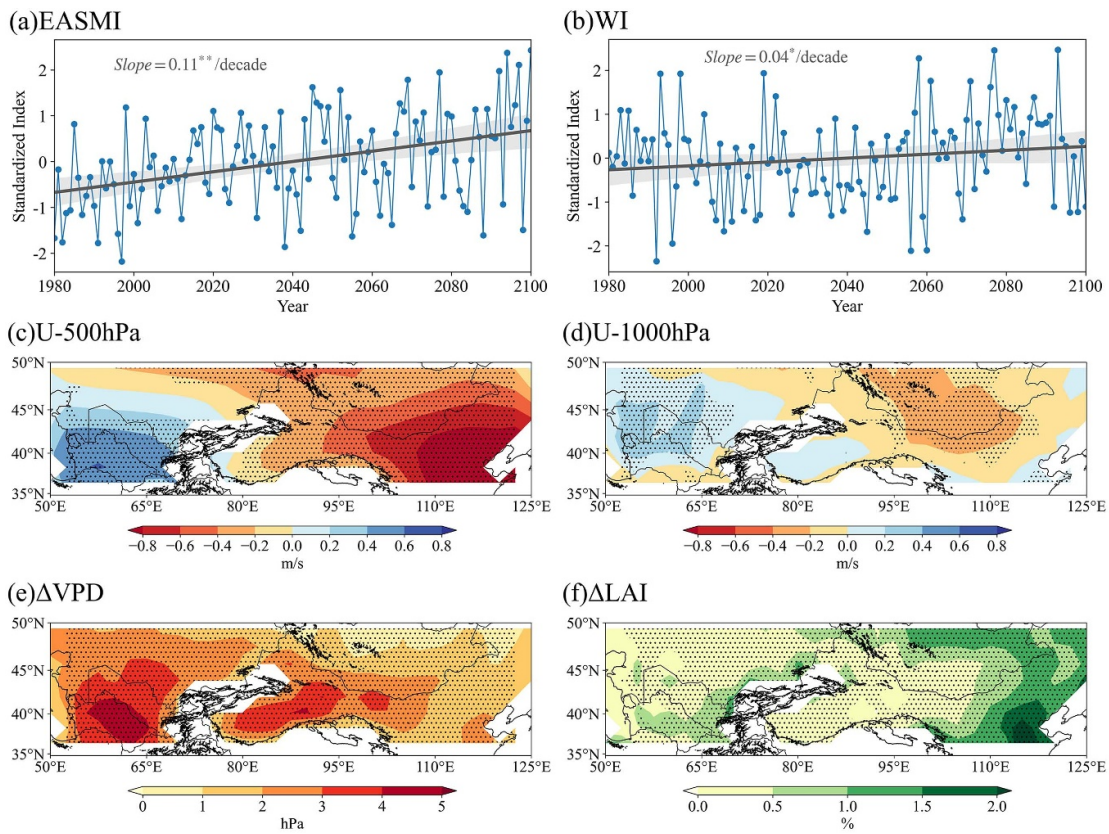


Figure 3. Mechanisms of the non-SM effects on precipitation and evapotranspiration in Central Asia and East Asia. (a), (b) The standardized time series of global weighted average East Asian summer monsoon index (EASMI) and westerly index (WI) from 1980 to 2100 in the six LFMIP-pdLC models. Trends significant at the 99% and 90% levels are marked with two asterisks and one asterisk, respectively. The shaded area indicates the 95% confidence interval of the line. (c) The spatial distribution of the simulated multi-model mean change in 500 hPa eastward wind (ΔU-500 hPa) between the historical period (1980–2014) and the SSP585 future period (2066–2100) across the six LFMIP-pdLC models. (d)–(f) The same as (c) but for 1000 hPa eastward wind (ΔU-1000hPa), vapor pressure deficit (ΔVPD) and leaf area index (ΔLAI), respectively. The dotted areas in (c)–(e) indicate that the sign of changes in ΔU-500 hPa, ΔU-1000hPa and ΔVPD aligns with the sign of changes in the multi-model average (as shown in the figure), and this consistency is maintained in at least four out of six models. In (f), stippling indicates agreement in the sign of ΔLAI change with the multi-model mean in at least 2 of the 3 models providing LAI data (CESM2, CMCC-ESM2, MPI-ESM1-2-LR).

Taken together, these results suggest that the non-SM effect influences *P–E* through different pathways in the two regions. In Central Asia, strengthened westerlies and higher VPD both favor increases in precipitation and evapotranspiration, but the evapotranspiration increase is larger, leading to a decrease in *P–E*. In contrast, in East Asia, the intensified EASM and increased greening (higher LAI) jointly promote precipitation and evapotranspiration, with the increase in precipitation being more dominant, thereby elevating *P–E*. These divergent changes shape the spatially heterogeneous pattern of *P–E* between the two regions.

4. Conclusion and discussion

Despite recognition of *P–E*'s spatial heterogeneity at a global scale (Hu *et al* 2025a), its fine-scale variation and underlying mechanisms within complex, populous regions like the East Asian and Central Asian drylands are poorly quantified—particularly against the backdrop of global warming, in which the warming and wetting trend in Northwest China has become a focal issue, and the East Asian drylands serve as the core areas of this trend. In this study, we adopted a model comparison framework that contrasts fully coupled CMIP6 simulations with land-only LFMIP-pdLC experiments with prescribed SM conditions. Our results reveal that *P–E* exhibits pronounced spatial heterogeneity between Central Asia and East Asia. Specifically, the spatial pattern of *P–E* is primarily driven by non-SM effect, while SM effect exerts a mitigating influence. This understanding allows us to construct a conceptual diagram of the underlying processes (figure 4). In Central Asia, non-SM effect promotes an increase in evapotranspiration via elevated VPD and precipitation through a strengthened WI. The increase in evapotranspiration is more pronounced, thereby exacerbating a local decline in *P–E*. Concurrently, SM effect counteracts this trend by reducing more evapotranspiration and promoting moisture convergence through decreased SM, which mitigates the reduction in precipitation and thus elevates P-E. However, the net impact of SM effect on *P–E* is smaller than that of non-SM effect,

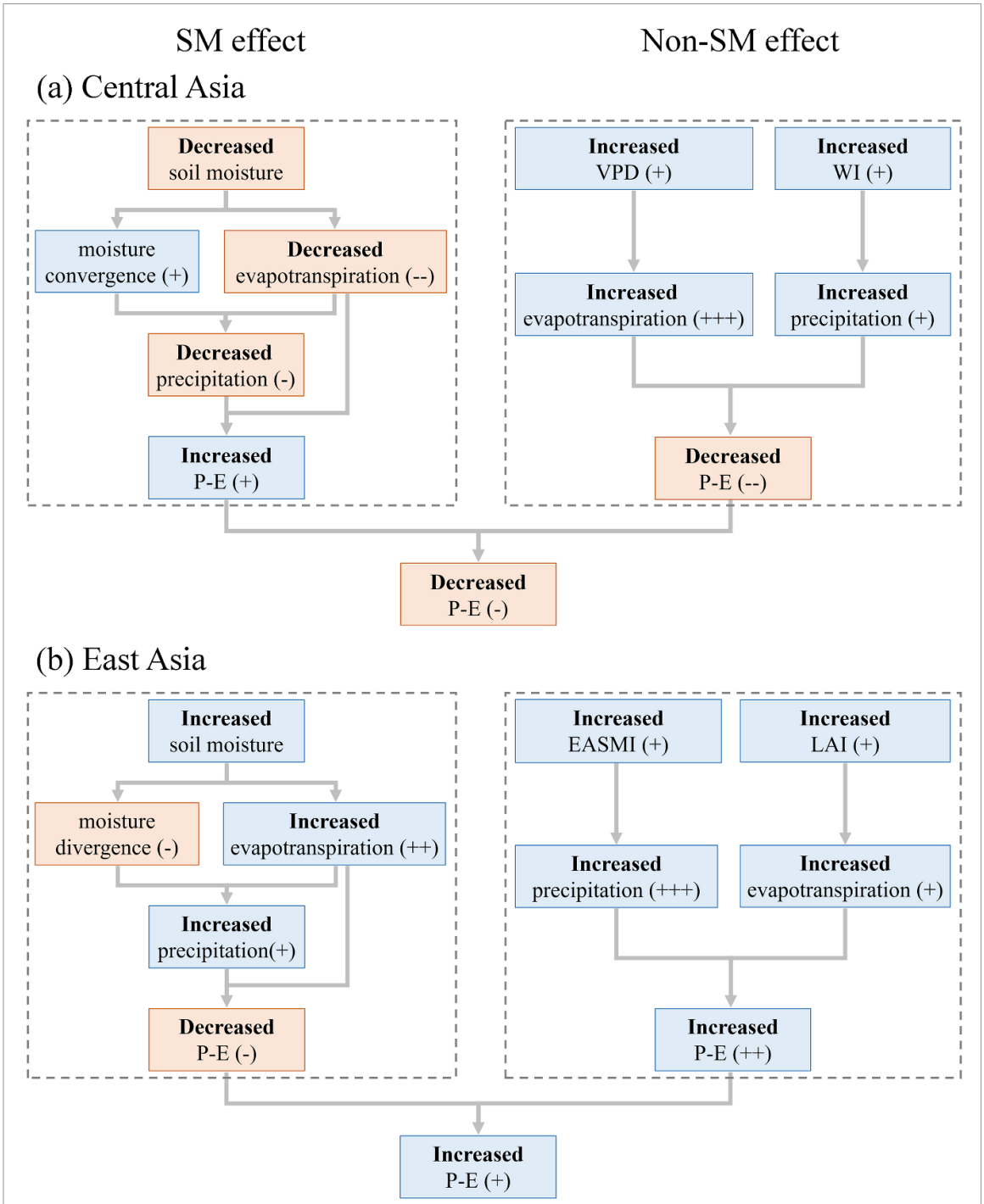


Figure 4. Conceptual representation of non-SM effect and SM effect on surface water availability in Central Asia and East Asia. (a) Central Asia: Soil desiccation elevates *P–E*, but non-SM effect exerts a stronger depressive influence, leading to a net decrease in *P–E*. (b) East Asia: Soil moistening suppresses *P–E*, yet non-SM effect provides a stronger amplification, resulting in a net increase in *P–E*.

resulting in an overall decrease. Conversely, in East Asia, non-SM effect enhances precipitation via an intensified EASMI and evapotranspiration through an increased LAI. Here, precipitation shows a more substantial increase, promoting a rise in local *P–E*. Within this region, an increase in SM further amplifies evapotranspiration and enhances moisture divergence. This leads to an even greater increase in evapotranspiration, which subsequently promotes precipitation, thereby reinforcing the decrease in *P–E*. Nonetheless, as in Central Asia, the SM effect remains secondary to the dominant non-SM effect, resulting in a net increase in *P–E* over East Asia—the core area of Northwest China's warming and wetting trend.

These results highlight that non-SM processes dominate the large-scale contrast in hydroclimatic

change across the drylands of Central and East Asia, while SM feedback serves as a buffering mechanism that reduces the magnitude of this contrast. In this sense, SM does not fundamentally alter the spatial pattern of *P–E* change, but it plays an important regulatory role in regional land-atmosphere coupling by modulating evapotranspiration and moisture convergence. Such regulation is especially important in drylands, where even modest shifts in *P–E* can lead to substantial hydrological and ecological consequences.

The regional implications of these findings are considerable. In the drylands of Central and East Asia, changes in *P–E* directly affect water availability, surface runoff, shallow groundwater recharge, oasis-desert interactions, grassland productivity, and the stability of irrigated agricultural systems. These changes, in turn, have direct consequences for food security, the livelihoods of farmers and herders, and the maintenance of ecological barrier functions such as windbreak and sand-fixation systems. By clarifying how SM and non-SM effects interact to shape *P–E*, this study deepens our understanding of dryland hydroclimatic processes and provides a scientific basis for assessing water-resource sustainability under climate change. More broadly, these findings offer useful support for adaptive water management, ecological conservation, and sustainable development across the drylands of the Silk Road Economic Belt (Olmstead 2014, Marques *et al* 2022, Scanlon *et al* 2023, Wang *et al* 2025).

Acknowledgments

This study is jointly supported by the National Science Foundation of China (42522503 and 42475023).

Data availability statement

The data that support the findings of this study are openly available at the following URL/DOI: https://esgf-node.ipsl.upmc.fr/projects/cmip6-ipsl/; https://www.plantplus.cn/doi/doi.org/10.6084.

Conflict of interest

The authors declare no conflict of competing financial interests.

Author contributions

Shanshan Wang 0000-0001-6373-8908
Conceptualization (equal), Supervision (equal), Writing – original draft (equal), Writing – review & editing (equal)

Yuanyuan Hu
Software (equal), Visualization (equal), Writing – original draft (equal)

Hao Wang
Conceptualization (equal), Investigation (equal), Methodology (equal)

Dongyu He
Investigation (equal)

Jianping Huang 0000-0003-2845-797X
Conceptualization (equal)

References

Abbott B W *et al* 2019 Human domination of the global water cycle absent from depictions and perceptions *Nat. Geosci.* **12** 533–40

Alessi M J, Herrera D A, Evans C P, DeGaetano A T and Ault T R 2022 Soil moisture conditions determine land-atmosphere coupling and drought risk in the northeastern United States *J. Geophys. Res.* **127** e2021JD034740

Allen R G, Pereira L S, Raes D and Smith M 1998 Crop evapotranspiration: guidelines for computing crop water requirements FAO irrigation and drainage paper 56 (Food and Agriculture Organization)

Bony S, Bellon G, Klocke D, Sherwood S, Fermepin S and Denvil S 2013 Robust direct effect of carbon dioxide on tropical circulation and regional precipitation Nat. *Geosci.* **6** 447–51

Chen X, Yuan L, Ma Y, Chen D, Su Z and Cao D 2024 A doubled increasing trend of evapotranspiration on the Tibetan Plateau *Sci. Bull.* **69** 1980–90

Cui A, Lu H, Liu X, Shen C, Xu D, Xu B and Wu N 2021 Tibetan Plateau precipitation modulated by the periodically coupled westerlies and Asian monsoon *Geophys. Res. Lett.* **48** e2020GL091543

Gu B, Zhou S, Yu B, Findell K L and Lintner B R 2025 Multifaceted changes in water availability with a warmer climate *npj Clim. Atmos. Sci.* **8** 31

Hu Y, Wang S, Guan X and Huang J 2025a Distinct effects of soil moisture on surface water availability in nearshore and inland drylands *Geophys. Res. Lett.* **52** e2025GL117631

Hu Y, Wang S, Wang H and Zhang J 2025b Enhanced response of surface water availability to soil moisture in humid regions under global warming *Clim. Dyn.* **63** 378

Hurk B V *et al* 2016 LS3MIP (v1.0) contribution to CMIP6: the land surface, snow and soil moisture model intercomparison project aims, setup and expected outcome *Geosci. Model Dev.* **9** 2809–32

Jiang K *et al* 2023 Combined influence of soil moisture and atmospheric humidity on land surface temperature under different climatic background *iScience* **26** 106837

Li M, Yao J and Zheng J 2024a Spatio-temporal changes in atmospheric aridity over the arid region of Central Asia during 1979–2019 *Ecol. Indic.* **169** 112814
Li X, Zhou Y, Han Z, Yuan X, Yi S, Zeng Y, Qin L, Lu M and Lu H 2024b Loess deposits in the low latitudes of East Asia reveal the ∼20 kyr precipitation cycle *Nat. Commun.* **15** 1023
Li Y, Ding Y and Li W 2017 Interdecadal variability of the Afro-Asian summer monsoon system *Adv. Atmos. Sci.* **34** 833–46
Li Y, Huang J, Ji M and Ran J 2015 Dryland expansion in northern China from 1948 to 2008 *Adv. Atmos. Sci.* **32** 870–6
Li Z, Sun Y, Li T, Ding Y and Hu T 2019 Future changes in East Asian summer monsoon circulation and precipitation under 1.5–5 °C of warming *Earth's Future* **7** 1391–406
Lin S, Chen X, Xia J, Xin Q, Fu Z, He B, Liu Q, Piao S and Yuan W 2025 Global vegetation production may decrease in this century due to rising atmospheric dryness *Nat. Ecol. Evol.* **9** 2279–89
Ma S, Chen S, Chen J, Chen J, Cao D, Xoplaki E, Luterbacher J, Chen F and Huang W 2025 The Holocene precipitation dipole pattern in the Asian drylands: mechanisms and processes from PMIP4 simulations and paleo-proxy evidence *Quat. Sci. Rev.* **347** 109091
Marques A C, Veras C E and Rodriguez D A 2022 Assessment of water policies contributions for sustainable water resources management under climate change scenarios *J. Hydrol.* **608** 127690
Middleton N J and Thomas D S G 1997 *World Atlas of Desertification* 2nd edn (Edward Arnold)
Olmstead S M 2014 Climate change adaptation and water resource management: a review of the literature *Energy Econ.* **46** 500–9
Qiao L, Zuo Z, Zhang R, Piao S, Xiao D and Zhang K 2023 Soil moisture-atmosphere coupling accelerates global warming *Nat. Commun.* **14** 4908
Sardans J, Miralles A, Tariq A, Zeng F, Wang R and Peñuelas J 2024 Growing aridity poses threats to global land surface *Commun. Earth Environ.* **5** 776
Scanlon B R *et al* 2023 Global water resources and the role of groundwater in a resilient water future *Nat. Rev. Earth Environ.* **4** 87–101
Seddon A W, Macias-Fauria M, Long P R, Benz D and Willis K J 2016 Sensitivity of global terrestrial ecosystems to climate variability *Nature* **531** 531229–32
Seo Y-W and Ha K-J 2022 Changes in land-atmosphere coupling increase compound drought and heatwaves over northern East Asia *npj Clim. Atmos. Sci.* **5** 100
Song F, Dong H, Wu L, Leung L R, Lu J, Dong L, Wu P and Zhou T 2025 Hot season gets hotter due to rainfall delay over tropical land in a warming climate *Nat. Commun.* **16** 2188
Trabucco A and Zomer R J 2008 Global aridity index and PET database V1 (Global_ai_PET_v1) (CGIAR-CSI Dataset)
Trabucco A and Zomer R 2019 Global aridity index and potential evapotranspiration (ET0) climate database v2 figshare dataset
Wang J and Wu Z 2024 Three types of East Asian summer rainfall associated with monsoon circulation and tropical cyclone activities: unique features and major influential factors *Clim. Dyn.* **62** 4099–116
Wang T, Fu Z, Zhang S and Li Z 2025 Water erosion risk assessment and predictive modelling for cultural heritage under climate change: a case study of the great Wall in the Yellow River basin, China *J. Clean. Prod.* **510** 145645
Wang Y and Yuan X 2022 Land-atmosphere coupling speeds up flash drought onset *Sci. Total Environ.* **851** 158109
Yang Y *et al* 2023 Evapotranspiration on a greening earth *Nat. Rev. Earth Environ.* **4** 626–41
Yuan W *et al* 2025 Impacts of rising atmospheric dryness on terrestrial ecosystem carbon cycle. *Nat. Rev. Earth Environ.* **6** 712–27
Yuan X, Yang K, Lu H, Sun J, Wang Y, Liu Y and Tang Q 2023 Weakened subtropical westerlies reduced early spring precipitation in the Southeast Tibetan Plateau *J. Clim.* **36** 4363–73
Zeng D, Yuan X and Roundy J K 2019 Effect of teleconnected land–atmosphere coupling on northeast China persistent drought in spring–summer of 2017 *J. Clim.* **32** 7403–20
Zhang Q, Yang J, Duan X, Ma P, Lu G, Zhu B, Liu X, Yue P, Wang Y and Liu W 2022 The eastward expansion of the climate humidification trend in northwest China and the synergistic influences on the circulation mechanism *Clim. Dyn.* **59** 2481–97
Zhang R P, Meng X H and Yang X Y 2025 Numerical simulation study on the influence of soil moisture heterogeneity on the convective initiation of a mesoscale convective system over the Tibetan Plateau *Plateau Meteorol.* **45** 1–16 (in Chinese)
Zhang Y *et al* 2023 Southern hemisphere dominates recent decline in global water availability *Science* **382** 579–84
Zhou S, Williams A P, Lintner B R, Findell K L, Keenan T F, Zhang Y and Gentine P 2022 Diminishing seasonality of subtropical water availability in a warmer world dominated by soil moisture–atmosphere feedbacks *Nat. Commun.* **13** 5752
Zhou S, Williams A P, Lintner B, Berg A M, Zhang Y, Keenan T F, Cook B I, Hagemann S, Seneviratne S I and Gentine P 2021 Soil moisture–atmosphere feedbacks mitigate declining water availability in drylands *Nat. Clim. Change* **11** 38–44
Zhu Q and Liu Y 2023 The combined effect of multiple water vapor transport channels can better reflect the variability in summer precipitation over North China *Clim. Dyn.* **61** 5887–904
Zomer R J, Xu J and Trabucco A 2022 Version 3 of the global aridity index and potential evapotranspiration dataset *Sci. Data* **9** 409